

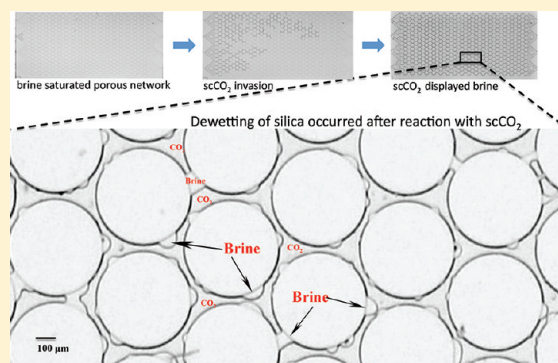
Dewetting of Silica Surfaces upon Reactions with Supercritical CO₂ and Brine: Pore-Scale Studies in Micromodels

Yongman Kim, Jiamin Wan,* Timothy J. Kneafsey, and Tetsu K. Tokunaga

Earth Sciences Division, Lawrence Berkeley National Laboratory, 1 Cyclotron Road, Berkeley, California 94720, United States

S Supporting Information

ABSTRACT: Wettability of reservoir minerals and rocks is a critical factor controlling CO₂ mobility, residual trapping, and safe-storage in geologic carbon sequestration, and currently is the factor imparting the greatest uncertainty in predicting capillary behavior in porous media. Very little information on wettability in supercritical CO₂ (scCO₂)–mineral-brine systems is available. We studied pore-scale wettability and wettability alteration in scCO₂–silica-brine systems using engineered micromodels (transparent pore networks), at 8.5 MPa and 45 °C, over a wide range of NaCl concentrations up to 5.0 M. Dewetting of silica surfaces upon reactions with scCO₂ was observed through water film thinning, water droplet formation, and contact angle increases within single pores. The brine contact angles increased from initial values near 0° up to 80° with larger increases under higher ionic strength conditions. Given the abundance of silica surfaces in reservoirs and caprocks, these results indicate that CO₂ induced dewetting may have important consequences on CO₂ sequestration including reducing capillary entry pressure, and altering quantities of CO₂ residual trapping, relative permeability, and caprock integrity.



1. INTRODUCTION

Geological CO₂ storage is one of the most promising methods to reduce anthropogenic CO₂ emissions into the atmosphere. Candidate geologic CO₂ storage sites are mainly deep saline aquifers, depleted oil and gas reservoirs, unmineable coal seams, and deep ocean sediments.^{1,2} Because of its lower density relative to water, containment of CO₂ within reservoirs requires prevention of its buoyant entry into and escape through overlying caprock (seal) formations. Wettability of reservoir rocks strongly influences CO₂ flow and distribution, and quantities of residual CO₂ trapping.^{3,4} Wettability of caprocks directly impacts the maximum injection pressure and storage height^{5,6} through altering the capillary breakthrough pressure. The capillary breakthrough pressure (P_{c,CO_2}) is the excess CO₂ phase pressure (relative to the brine phase) required to initiate CO₂ flow through geologic medium previously saturated with brine. Capillary breakthrough pressure of CO₂ can be estimated with the Young–Laplace equation

$$P_{c,CO_2} = \frac{2 \cdot \gamma_{w,CO_2} \cdot \cos \theta}{r} \quad (1)$$

where γ_{w,CO_2} is the interfacial tension (IFT) between CO₂ and the aqueous phase, θ is the contact angle of the aqueous phase on the mineral surface, and r is the characteristic radius of the pores controlling percolation of CO₂. The range of r is a local property of the geologic material, typically ranging from a few to hundreds of μm in reservoirs, and in the nm range for caprocks. Values of γ_{w,CO_2} are relatively well constrained, being

between 20 to 35 mN m⁻¹ under the pressures, temperatures, and salinities associated with scCO₂ sequestration.^{5,7–10} Variations in θ have large consequences because increases toward 90° and greater lead to diminishing of P_{c,CO_2} and even its reversal, allowing spontaneous imbibition of CO₂ in absence of excess pressure. Measurements of θ are commonly obtained on macroscopic surfaces with droplet sizes typically in the range of a few mm. Wettability is also inferred from macroscopic measurements of capillary displacement (core flooding) of immiscible fluids. However, direct measurement of wettability within porous media remains challenging. Therefore wettability is currently the factor imparting the greatest uncertainty in predicting capillary behavior in porous media.

Injected CO₂ is usually assumed to behave as a nonwetting fluid in geological formations (water-wet). However, this assumption was recently questioned, and partial wetting of CO₂ on mineral surfaces has been investigated by several groups.^{8,11–16} Although wettability change has significant implications, there is still a paucity of data addressing this phenomenon under geological CO₂ storage conditions, particularly at the pore-scale.

Silica–CO₂ interactions have been studied through laboratory experiments^{17–24} and molecular simulations.^{20,25,26} For example, Dickson et al. investigated contact angle changes

Received: November 16, 2011

Revised: March 9, 2012

Accepted: March 11, 2012

Published: March 11, 2012

when CO₂ reacts with silanol groups on modified silica surfaces.¹⁹ Tripp and Combes showed through infrared spectroscopy that CO₂ removes (deuterated) water from silica surfaces more effectively than organic solvents, and that CO₂–silica interactions were limited to physisorption even after complete dehydration.²¹ McCool and Tripp reported that the reacted scCO₂ with silica hydroxyls could not be removed from the silica surface by simple evacuation.²² Cole et al. studied the interaction of scCO₂ in nanoscale pores of shale and reported that scCO₂ may interact with muscovite hydroxyl groups resulting in significant decrease of its mobility.²⁰ Vishnyakov et al. studied the interactions between scCO₂ and silica nanoparticles using molecular simulations, and reported that scCO₂ strongly reacts with hydroxyl groups on the silica surface via hydrogen bonds.²⁵ Complications in contact angle measurements associated with potential surface contamination can add significant uncertainty.^{27,28} These findings indicate that scCO₂ may alter the wettability of silica surface, and also that scCO₂ becomes the partially wetting phase as pressure increases. However, these previous studies did not provide direct evidence of wettability changes within pores.

Micromodels are transparent pore networks used for laboratory studies of microscopic distribution and transport of fluids in porous media²⁹ in many different applications including research related to oil recovery from reservoirs,^{30–32} nonaqueous phase liquid dissolution,^{33–36} and colloid transport.^{37–42} Few micromodel experiments have been conducted under elevated pressure and temperature,^{8,30,43–50} and even fewer have been conducted under supercritical scCO₂ conditions. Chalbaud et al. investigated distributions of CO₂ and water in glass micromodels having different wettabilities.⁸ Zhang et al. studied CO₂ and water displacement in a micromodel with dual-permeability pore size distributions.⁴⁶ Riazi et al. observed displacement behavior indicating that CO₂ injected into depleted oil reservoirs may have faster breakthrough relative to injection into aquifers of similar pore geometry.⁴⁷ Er et al. visually analyzed CO₂ and oil interactions near the fracture region inside a micromodel matrix.⁴⁹ Despite their versatility, limitations common to most micromodels include intrinsic restriction to two-dimensional pore networks of uniform etch depth, relatively uniform surface chemistry (silica glasses or organic polymers), relatively smooth surface microtopography, and lack of pore sizes finer than about 10 μm. To the best of our knowledge, quantitative studies addressing wettability alteration at the pore-scale under supercritical scCO₂ conditions have yet to be reported.

The objective of this study is to understand if, and to what extent, interactions with scCO₂ change the wettability of silica, the most common reservoir solid. We utilized transparent engineered silica micromodels to study the wetting behavior of scCO₂ through direct visualization of the phase displacement processes, and measurement of contact angle alterations, at the pore-scale under conditions relevant to geological CO₂ storage.

2. METHOD

2.1. High Pressure Microscopy/Micromodel System.

An inverted microscope (Carl Zeiss, Observer Z1.m) was used for viewing, with images recorded using a CCD camera (Carl Zeiss, AxioCam MRc5) connected to a computer. The micromodel was placed horizontally on the custom-designed stage of the microscope. Brine (CO₂-free) was filled into the micromodel using a stainless steel syringe (KD scientific, 2.5 mL with 1/16 in. Swagelok fitting) controlled with a precision

syringe pump (Harvard, PHD 2000). A precision, high-pressure syringe pump (Teledyne ISCO, 500HP) was used to fill scCO₂ (presaturated with water) into the micromodel. To prepare scCO₂, a commercial CO₂ cylinder (Airgas, 99.99%) equipped with an eductor tube was connected to the ISCO pump. The prepared scCO₂ was presaturated with water at 8.5 MPa 45 °C in a stirred reactor (Parr, model 4560). Pressure was measured with a pressure transducer (Omega, PXM01MD0-400BARGV). The system was contained in an insulated enclosure, heated with a forced convection heater and heating tape, controlled with PID controllers (Cole Parmer, EW-89000-10) connected to thermocouples (Omega, Type T). Additional description of the experimental system and a schematic diagram are provided in Figure S1 in the Supporting Information (SI).

2.2. Micromodel. The high-pressure micromodels used in this study were fabricated by Micronit Microfluidics BV. These were made out of fused silica plates (Schott Lithotec, Lithosil Q1), with homogeneous pore network patterns etched on the fused silica plates with hydrofluoric acid. Two symmetrically patterned plates were fused together to form a homogeneous 2-dimensional porous network having a patterned area of 20 mm × 10 mm, composed of 576 discoid silica grains (590 μm diameter). Two different homogeneous patterns were used for the current work, with calculated pore volumes (PV) of 0.31 and 0.89 μL (pattern parameters are described in the SI). The top (plan view) and cross-section images of the micromodel are shown in Figure S2 in the SI. A unique feature of the micromodel pattern is that the grains do not contact each other (unlike the real porous media). This design minimizes accumulation of residual water in pendular structures between grains, and allows clearer observations of the water layer and wettability changes, and facilitates contact angle measurements.

2.3. Experiment Procedures. Sodium chloride brines (0.01 to 5.00 M) were prepared with deionized (DI) water (Barnstead, NanoPure) and NaCl (Sigma-Aldrich, ACS reagent grade). The pH values of the brines were between 5.8 and 6.2 depending on ionic strength. Brines were degassed and stored at room temperature under vacuum until being used. Micromodels were cleaned before usage by injecting 5 mL of absolute ethanol (Mallinckodt Baker, ACS reagent grade) followed by 20 mL of DI water, then dried at 120 °C for 24 h in a drying oven. After the clean micromodel was assembled in the experimental system, vacuum was applied for 3 h at 45 °C in order to remove residual air inside the micromodel and the flow lines. All components directly connected with the micromodel were kept inside the thermal insulation chamber (SI, Figure S1) to maintain a temperature of 45 ± 1 °C during experiments. Degassed brine was then injected into the micromodel until the flow lines and the micromodel were fully saturated. The system was then gradually pressurized with the syringe pumps up to 8.5 MPa over a period of 30 min. So far the prepared water-saturated scCO₂ was kept isolated from the brine. For the scCO₂ and the brine to reach thermal equilibrium, the system was equilibrated at 45 °C for 3 h, then the brine drainage process (scCO₂ invasion) was initiated. The syringe pump on the brine side (Harvard) withdrew brine at a constant flow rate (4 μL min⁻¹ for 20 min), and the pump on the scCO₂ side (ISCO) injected the scCO₂ at constant pressure. A total 90 PV of scCO₂ was injected during the brine drainage process. Upon completion of the drainage the inlet and outlet of the micromodel were closed off, and the system was then equilibrated at the same pressure and temperature. Images of scCO₂ and brine distributions in the micromodel were

recorded throughout and after the drainage process. To avoid procedure-dependent results (different reaction history of the silica surfaces with scCO₂ could potentially complicate interpretation of results), a new micromodel was used for each experiment.

To isolate the effects caused by surface reactions with CO₂, an experiment using air as the nonwetting fluid was conducted at atmospheric pressure. The micromodel was saturated with DI water and then air was injected at 8 μL min⁻¹ for 15 min under ambient pressure and temperature. Images of fluid phase distributions in the water–air system were recorded using the same method described above.

2.4. Image Analyses. ImageJ software⁵¹ combined with a contact angle plug-in (Marco Brugnara, marco.brugnara@ing.unitn.it) was used to analyze the acquired images. The shape of the silica grains on the imaging plane is circular, thus contact lines of the brine droplets are curved rather than flat. Therefore the curved wetting surface must be accounted for when determining intrinsic contact angles (the equivalent angle expected if the brine droplet is deposited on a flat surface of the same composition). Details of the analysis procedure and discussion about contact angles on curved surfaces can be found in the work of Extrand and Moon⁵² and Marmur and Krasovitski.⁵³ Some example images of the contact angle measurement process with ImageJ are shown in the SI.

3. RESULTS AND DISCUSSION

3.1. Air as the Nonaqueous Fluid Phase: The Control Experiment. This experiment was conducted to understand the wetting behavior of the silica pore walls of the micromodels when air is the nonaqueous phase. The experimental procedures and conditions were the same as those used with CO₂ as the nonaqueous phase, except that the total pressure was 0.1 MPa. Representative images taken at the end of the water drainage (air displaced water in the pore spaces) are shown in Figure 1. After drainage, the residual water remained as thick films between the silica grains and air. To visually record the existence of water films, we imposed a steady flow of air to impart shear stress at air–water interfaces. The airflow pushed the water films to accumulate as bulges along the downstream sides of the silica grains, with advancing contact

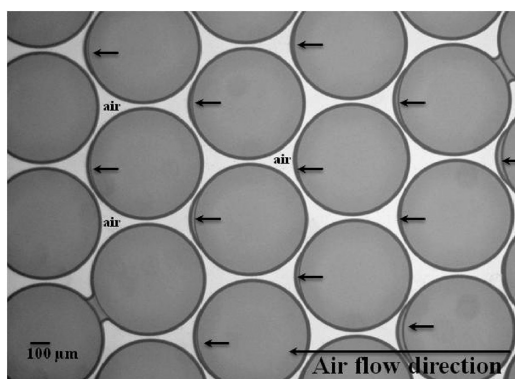


Figure 1. Images of residual water residing as thick water-films coated on the silica grains after air displaced water from the pore space. The dynamic contact angles (measured $11.5^\circ \pm 1.6^\circ$) are formed by the airflow. Upon stopping the airflow the advancing contact angles disappeared (near zero contact angles under static condition). The silica micromodel is strongly hydrophilic when air is the nonaqueous phase.

angles up to 12° . Upon stopping airflow, the water bulges retracted back into thick water films with static contact angles near 0° . This demonstrated that the silica micromodel is strongly hydrophilic when air is the nonaqueous fluid phase.

3.2. scCO₂ As the Nonaqueous Fluid Phase. Figure 2 shows representative images taken during the drainage of 1 M NaCl brine displaced by scCO₂ at 8.5 MPa and 45 °C. The micromodel was set vertically and the scCO₂ was injected from the bottom to the top at the rate of 4 μL/min for 20 min. These images were taken directly by using a digital camera (Nikon D90, 12.3 Megapixel) in order to view the entire pore network of the micromodel, instead of using the CCD camera through the microscope (for individual pores). The photographs show how the scCO₂ flow paths developed over time, and the time-dependent saturation distributions. The phase saturation can be quantitatively determined from the images, and many other studies can be done using this method. Although gravity influences flow paths and the spatial distribution of phases, it does not affect surface wetting properties that are of primary interest in this study.

During and after the drainage (scCO₂ injection) process described in the previous paragraph, we observed dewetting of silica surfaces through water-film thinning, formation and growth of water droplets, and contact angle increase. Figure 3 shows the water droplets formed during and after the drainage. The photograph was taken 2 h after initiating the drainage process, when the droplet sizes, shapes, and contact angles had reached apparent steady state (based on analyzing the continuous video recording). The contact angles of the brine droplets increased up to 80° . The originally water-wet (with near zero contact angles in Figure 1) silica grains became intermediate wet after reaction with scCO₂ in brine. Sketches of the cross section of a single pore (Figure 4) can help us to better understand the dewetting process. The bottom left figure shows a brine-filled hydrophilic pore. The silica was initially hydrophilic, as demonstrated in Figure 1. Then the brine was drained by injection of the water-saturated scCO₂, after which the capillary-trapped residual brine resided as a smooth thick film between the silica and scCO₂ (the bottom middle figure). Upon scCO₂ interaction with the brine and the silica, the water-wettability of the silica decreased, and minimization of the scCO₂-brine capillary interfacial surface area redistributed most the residual water into “corners” of pores. In the recorded images, the redistributed residual water appears as droplets along grain surfaces. In 3-dimensional porous media, the dewetting would drive the excess water into pendular rings among grain–grain contacts, and into local microtopographic minima along rough grain surfaces.

3.3. Time Dependence of Contact Angles Change. Upon displacement of brine by scCO₂, changes of residual water configuration on silica grain surfaces were observed only over a short time period. Images of water droplet growth during the drainage process with 0.01 M NaCl are shown in Figure 5. The image capture rate for the microscope camera was 0.45 s frame⁻¹, and a small field of view was monitored for 2 h. Water droplet growth was only observed over about a 20 s period during monitoring. This may be mainly because of the narrow monitoring field of view (locations of droplet growth cannot be predicted and preselected for monitoring). In Figure 5, the “0 s” image was captured 1 s prior to the image showing appreciable water droplet growth. Times shown in other images are relative to 0 s. Whereas the size of the brine droplets gradually increased over the time, the apparent contact angle

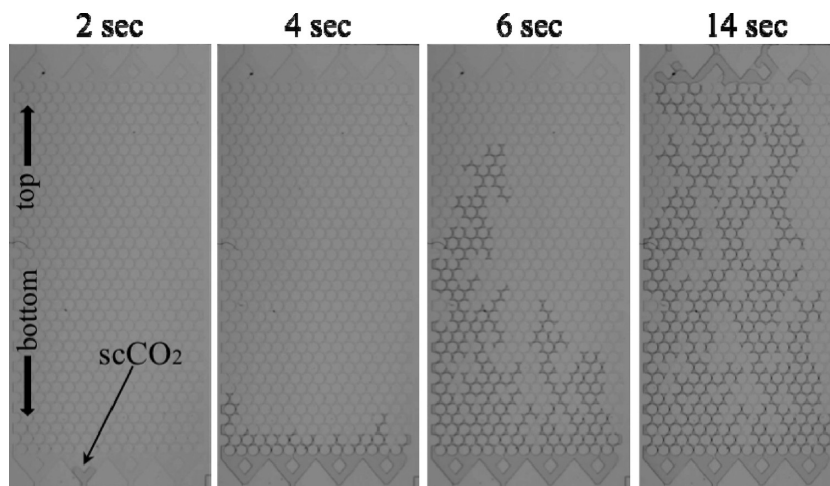


Figure 2. Selected images during brine drainage at 8.5 MPa and 45 °C. Supercritical CO₂ was injected at 4 μL/min for 20 min, at the bottom. The pore space was initially saturated with brine (1 M NaCl) then displaced with scCO₂. After 100 PV of scCO₂ injection, about 85% of the brine was displaced.

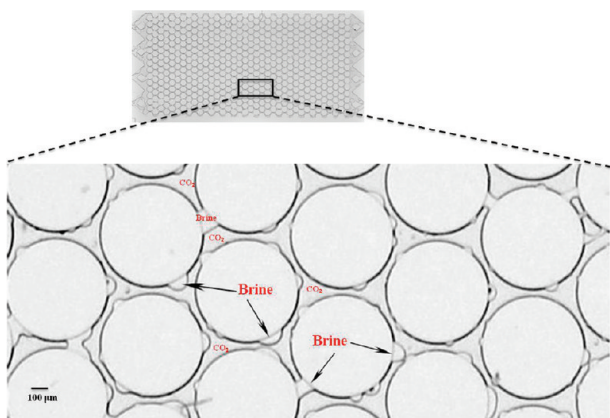


Figure 3. Dewetting of silica surfaces occurred upon reaction with scCO₂, shown by formation of water-droplets and increased contact angles. The raw microscope image was taken 2 h after the drainage process at 8.5 MPa and 45 °C with 1 M NaCl brine. The equilibrium contact angles of water-droplets are in the range of 40° to 80°.

did not change significantly after the observed initial droplet formation. Apparently, most of the dewetting occurred quickly after scCO₂ entered pores, within the time frame of seconds.

3.4. Effect of Ionic Strength. To understand effects of ionic strength on wetting behavior of the scCO₂–brine–silica system, experiments were conducted with 0.01, 1.0, 3.0, and 5.0 M NaCl solutions. Figure 6 shows the effect of ionic strength on wettability at equilibrium following brine drainage. The darker areas between the circular grains are water droplets and the brighter areas are scCO₂. Note that the lines between the brine droplets and the silica grains are thinner than those between scCO₂ and silica grains, because of the different refractive indices (RI) of the different materials. The reported RI of the fused silica is 1.458 (provided by the manufacturer), brine is 1.391,⁵⁴ and scCO₂ under our experimental pressure and temperature is 1.088.⁵⁵ The RI difference between the water and the silica is smaller than that between scCO₂ and silica. Example images of the contact angle measurement process using ImageJ software are shown in Figure S2 of the SI.

We measured contact angles of 15 randomly selected brine droplets (easier to measure ones) from each ionic strength condition. Contact angle values, averages, sample variances, and

t test analyses are presented in Table S2, and the data are summarized below. Note that the dewetting phenomena we observed are reproducible, but we do not expect the exact values of the contact angles to be reproducible at any specific location. The measured contact angles of the droplets are in the range of 50°–75° (mean value = 66°) for 1 M NaCl, 55°–76° (mean value = 65°) for 3 M NaCl, and 66°–87° (mean value = 75°) for 5 M NaCl. Contact angles for the 0.01 M NaCl condition were clearly smaller from the images. However, few droplets had contact angles over 60°. The measured data 37°–68° (mean value = 54°) only represent this group of larger ones. These data suggest that even in this otherwise homogeneous micromodel, variability in local wettability can be significant. The general trend (significant at *p* = 0.01) is that water wettability of silica surfaces decreases with increased salinity in the scCO₂–brine–silica system.

3.5. Nonaxisymmetric Brine-Droplets. Unlike conventional methods (e.g., sessile drop) for measuring contact angle, the droplets in micromodels are not axisymmetric. In micromodels the observed radius of curvature *R*₁ of any point along a droplet interface has its associated second principal radius *R*₂ on a plane orthogonal to the focal plane. Although this second principal radius cannot be imaged with conventional optical microscopy, it can be calculated. We assume that the contact angle *θ* measured on the microscope focal plane is equal to the contact angle in planes transecting observed radii of curvature and orthogonal to the view plane. If the pore depth *d*₂ is known, the associated pore radius *R*₂ is simply half the pore depth, such that the second radius of curvature *R*₂ = *d* / (2cos*θ*). The differential (capillary) pressure in the droplet relative to the nonwetting phase can then be calculated with the Young–Laplace equation expressed as

$$\Delta P = \gamma_{w,CO_2} \left(\frac{1}{R_1} + \frac{2\cos\theta}{d} \right) \quad (2)$$

Assuming local equilibrium between the capillary and adsorbed water,^{56,57} eq 2 can be used to estimate lower magnitudes of disjoining pressures^{58,59} in residual water films. The magnitude of ΔP in our systems ranged up to about 10 kPa, with larger values associated with smaller *R*₁ and small *θ*. Equation 2 also

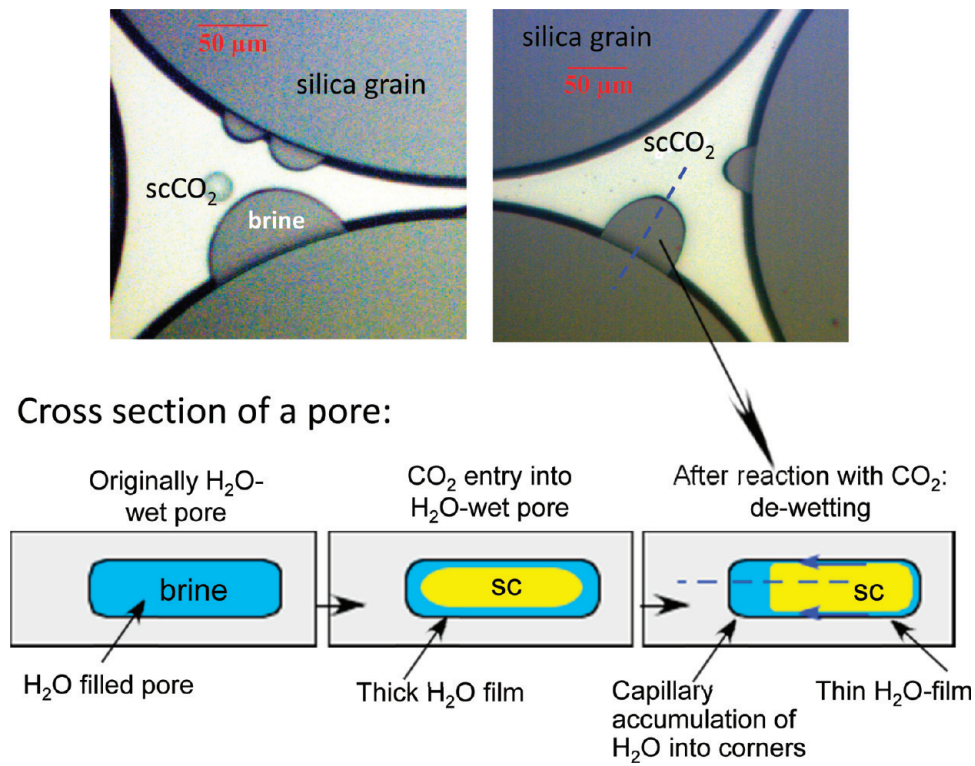


Figure 4. Dewetting process in a pore. Two raw images of single pores from the micromodels are shown in the upper section. Sketches of the cross-section of a pore are shown in the lower part. The pore was initially saturated with water (left). Immediately after the $scCO_2$ displaced the water, the residual water resided as a smooth thick film between the hydrophilic silica and $scCO_2$ (middle). Upon reactions with $scCO_2$ and the brine, the silica surface became less water wettable, resulting in water film thinning and water accumulating in the corners (right), where the interfacial area of the free brine– $scCO_2$ interface is minimized. Viewed from the top, this residual water appears as water droplets.

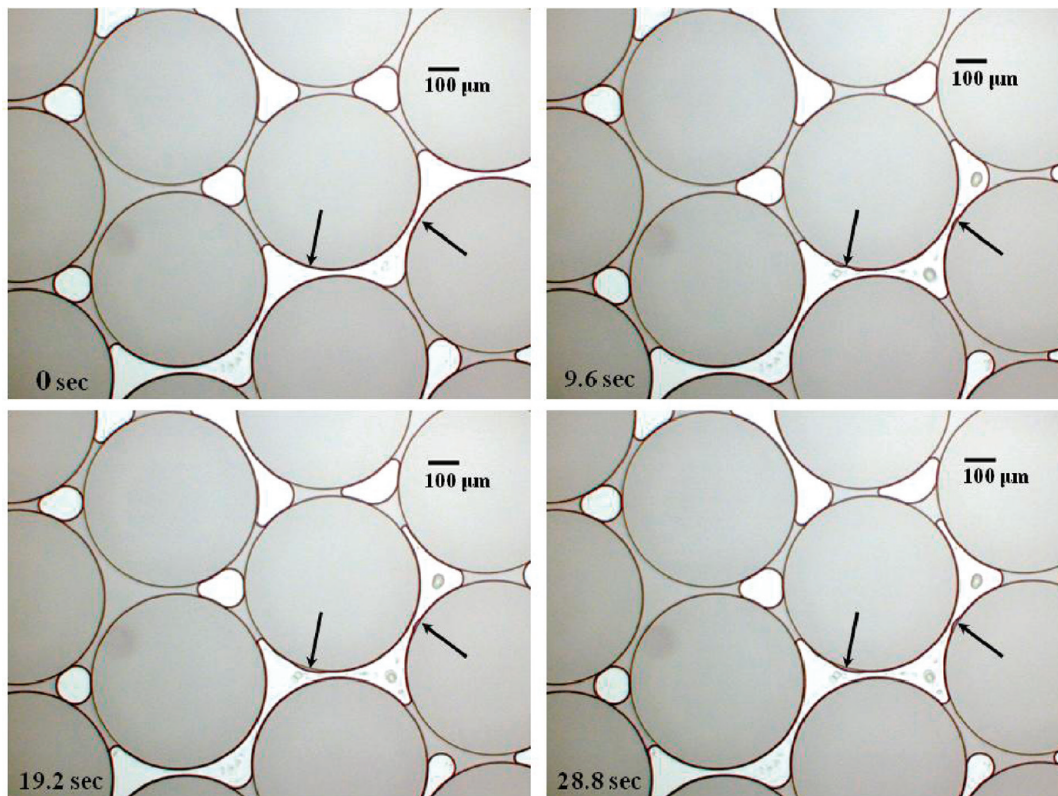


Figure 5. Raw microscope photograph images of water droplet growth during drainage under conditions of 0.01 M NaCl, 8.5 MPa, and 45 °C. The $scCO_2$ appears as lighter colored regions. The water droplets (indicated by arrows) are growing on the silica grains during the drainage.

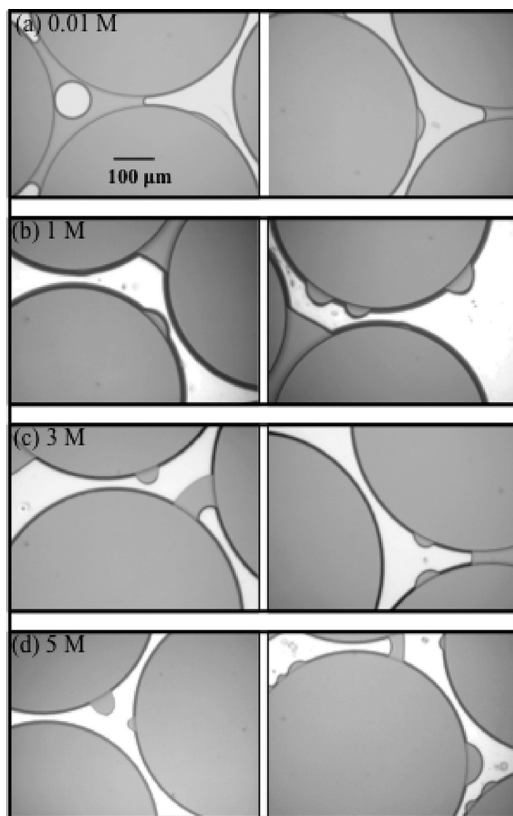
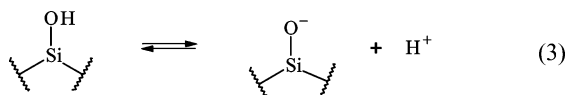


Figure 6. Effect of ionic strength on wetting. The raw microscope images show equilibrium contact angles of water droplets on silica grains after the drainage process at 8.5 MPa and 45 °C. The injected scCO_2 is light in color.

indicates that droplets with different combinations of θ and R_1 can be in capillary pressure disequilibrium.

3.6. Mechanisms Responsible for Dewetting. The ability of water to remain attached to a mineral surface (wettability) results from intermolecular interactions among the three phases: the mineral, and aqueous and nonaqueous fluids. The main chemical groups on silica surfaces in aqueous solutions are silanol and silicic acid groups.⁶⁰ The hydrophilicity of silica depends on the surface density of these functional groups. At near neutral pH, some silica surfaces are negatively charged through deprotonation of silanol sites as in Reaction 3 below. The measured pK_a values for Reaction 3 are in the range of 5.7 and 7.7.⁶¹ When scCO_2 dissolves into brine, the brine pH becomes about 3.0.⁶² Thus Reactions 3 shift to the left, and the surface charge of silica is diminished.



The pH effect on silica wettability reported by Gribanova was that when pH is decreased from 6 to 3, contact angle increased from 19° to 23° in the air–brine–silica system at ambient pressure and temperature.⁶³ Chiquet et al. explained that the decreased surface charge with decreased pH results in destabilizing the water film, therefore increasing contact angles.¹¹ Other factors besides pH-dependent surface charge may also contribute to explain the magnitude of the measured wettability changes through reaction with scCO_2 . Recently, Puah et al. studied the effect of surface charge on wettability and wetting kinetics by measuring contact angles on a coated

titania surface.⁶⁴ They analyzed the experimental results using molecular-kinetic theory and concluded that surface charge affects both the static and dynamic wettability. Dickson et al. proposed that the reaction between CO_2 and the silanol group is physisorption capping of the silanol groups providing an additional mechanism to explain the increased contact angle.¹⁹ Based on infrared spectroscopy of direct scCO_2 –silica interactions, Tripp and Combes concluded that the physisorption was weak.²¹ Vishnyakov et al. reported that scCO_2 can strongly react with hydroxyl groups on silica substrates via hydrogen bonds.²⁵ The electric double layer within high ionic strength films on acidic silica surfaces is predicted to become highly compressed because of the very low surface charge density being balanced over short (nm) distances.⁶⁵ Although research on mechanisms responsible for wettability change in systems like ours is ongoing, it is clear that reactions with scCO_2 reduce the wettability of silica surfaces.

We also observed increased contact angles as brine salinity increases, consistent with Sghaier et al.,⁶⁶ who found increased contact angle with increased NaCl concentration on hydrophilic surfaces. Ion exclusion at water–fluid interfaces with increased salinity^{67–70} increases the scCO_2 /brine IFT^{7,8} and contributes to contact angle increases. The reduced film thickness from compression of the electric double layer may permit greater scCO_2 reaction with silica, resulting in decreased energy of its surface. If the IFT of brine/silica and of scCO_2 /silica are independent of salinity (or the dependence is negligible), then the contact angle increase may largely correspond to the increased IFT of scCO_2 /brine. However, quantitative relations between the IFTs and contact angles in various brine concentrations have not yet been reported.^{11,71} Our investigation on contact angle salinity dependence in scCO_2 –brine–mineral systems is in progress.

4. IMPLICATIONS

In reservoirs used for geological CO_2 sequestration, the injected CO_2 will inevitably interact with reservoir minerals. The present work provides an improved understanding on the wetting behavior of CO_2 under deep reservoir conditions, showing that CO_2 cannot be treated as a simple nonwetting fluid in reservoir pores. Supercritical CO_2 can react quickly (within seconds) with silica resulting in dewetting of the silica surface. The process of dewetting, water-film thinning, water droplet formation, and contact angle increase were visualized in our micromodels. The contact angle on silica increased from initially near 0° up to 80°, depending on ionic strength. The higher ionic strength results in larger contact angles. Given the abundance of silica surfaces in the subsurface, these results imply that CO_2 injection-induced dewetting may have important consequences on CO_2 sequestration, including determining CO_2 residual saturation (a major trapping mechanism), CO_2 flow paths and relative permeability (mobility), and capillary entry pressure (injectivity and caprock integrity). We do not yet know if the dewetting phenomenon observed on silica also occurs on other mineral surfaces. Although two-dimensional micromodels have their limitations as representations of natural porous medium, they permit the spatial and temporal resolution required for investigating critical pore scale phenomena such as wettability and capillary entry.

■ ASSOCIATED CONTENT

● Supporting Information

Table S1, parameters of the engineered micromodels; Table S2, Contact angle measurements of selected 15 brine droplets from each micromodel experiment; Figure S1, schematic diagram of the high pressure microscopy system; Figure S2, Photograph of the micromodel plan view and cross section; and Figure S3, example images of contact angle measurement with ImageJ software. This material is available free of charge via the Internet at <http://pubs.acs.org>.

■ AUTHOR INFORMATION

Corresponding Author

*Phone: 1-510-486-6004; fax: 1-510-486-7152; e-mail: jwan@lbl.gov.

Notes

The authors declare no competing financial interest.

■ ACKNOWLEDGMENTS

We sincerely thank the four anonymous reviewers and associate editor Dr. Dzombak for their insightful and constructive comments and suggestions. This material is based upon work supported as part of the Center for Nanoscale Control of Geologic CO₂, an Energy Frontier Research Center funded by the U.S. Department of Energy, Office of Science, Office of Basic Energy Sciences under Award Number DE-AC02-05CH11231.

■ REFERENCES

- (1) Intergovernmental Panel on Climate Change. Working Group III. *IPCC Special Report on Carbon Dioxide Capture and Storage*; Cambridge University Press, for the Intergovernmental Panel on Climate Change: Cambridge, 2005; p x, 431 p.
- (2) Shukla, R.; Ranjith, P.; Haque, A.; Choi, X. A review of studies on CO₂ sequestration and caprock integrity. *Fuel* **2010**, *89* (10), 2651–2664.
- (3) Saadatpoor, E.; Bryant, S. L.; Sepehrnoori, K. New Trapping Mechanism in Carbon Sequestration. *Transp. Porous Media* **2010**, *82* (1), 3–17.
- (4) Krevor, S. C. M.; Pini, R.; Li, B. X.; Benson, S. M. Capillary heterogeneity trapping of CO₂ in a sandstone rock at reservoir conditions. *Geophys. Res. Lett.* **2011**, *38*.
- (5) Li, Z. W.; Dong, M. Z.; Li, S. L.; Huang, S. CO₂ sequestration in depleted oil and gas reservoirs - caprock characterization and storage capacity. *Energy Convers. Manage.* **2006**, *47* (11–12), 1372–1382.
- (6) Naylor, M.; Wilkinson, M.; Haszeldine, R. S. Calculation of CO₂ column heights in depleted gas fields from known pre-production gas column heights. *Mar. Petrol. Geol.* **2011**, *28* (5), 1083–1093.
- (7) Bachu, S.; Bennion, D. B. Interfacial Tension between CO₂, Freshwater, and Brine in the Range of Pressure from (2 to 27) MPa, Temperature from (20 to 125) degrees C, and Water Salinity from (0 to 334 000) mg(.)L(-1). *J. Chem. Eng. Data* **2009**, *54* (3), 765–775.
- (8) Chalabaud, C.; Robin, M.; Lombard, J. M.; Martin, F.; Eggermann, P.; Bertin, H. Interfacial tension measurements and wettability evaluation for geological CO₂ storage. *Adv. Water Resour.* **2009**, *32* (1), 98–109.
- (9) Chiquet, P.; Daridon, J. L.; Broseta, D.; Thibeau, S. CO₂/water interfacial tensions under pressure and temperature conditions of CO₂ geological storage. *Energy Convers. Manage.* **2007**, *48* (3), 736–744.
- (10) Schulz, C.; Jaeger, P. T.; Eggers, R. Wettability of Reservoir Rock Materials in High Pressure Carbon Dioxide. The 11th International Symposium on Reservoir Wettability, University of Calgary, AB, Canada, September 6–9, 2010; University of Calgary, AB, Canada, 2010.

(11) Chiquet, P.; Broseta, D.; Thibeau, S. Wettability alteration of caprock minerals by carbon dioxide. *Geofluids* **2007**, *7* (2), 112–122.

(12) Yang, D. Y.; Gu, Y. G.; Tontiwachwuthikul, P. Wettability determination of the reservoir brine-reservoir rock system with dissolution of CO₂ at high pressures and elevated temperatures. *Energy Fuel* **2008**, *22* (1), 504–509.

(13) Siemons, N.; Bruining, H.; Castelijn, H.; Wolf, K. H. Pressure dependence of the contact angle in a CO₂-H₂O-coal system. *J. Colloid Interface Sci.* **2006**, *297* (2), 755–761.

(14) Espinoza, D. N.; Santamarina, J. C. Water-CO₂-mineral systems: Interfacial tension, contact angle, and diffusion-Implications to CO₂ geological storage. *Water Resour. Res.* **2010**, *46*, W07537.

(15) Jaeger, P. T.; Alotaibi, M. B.; Nasr-El-Din, H. A. Influence of Compressed Carbon Dioxide on the Capillarity of the Gas-Crude Oil-Reservoir Water System. *J. Chem. Eng. Data* **2010**, *55* (11), 5246–5251.

(16) Hildenbrand, A.; Schlomer, S.; Krooss, B. M.; Littke, R. Gas breakthrough experiments on pelitic rocks: Comparative study with N₂, CO₂ and CH₄. *Geofluids* **2004**, *4* (1), 61–80.

(17) Di Giovanni, O.; Dorfler, W.; Mazzotti, M.; Morbidelli, M. Adsorption of supercritical carbon dioxide on silica. *Langmuir* **2001**, *17* (14), 4316–4321.

(18) Roque-Malherbe, R.; Polanco-Estrella, R.; Marquez-Linares, F. Study of the Interaction between Silica Surfaces and the Carbon Dioxide Molecule. *J. Phys. Chem. C* **2010**, *114* (41), 17773–17787.

(19) Dickson, J. L.; Gupta, G.; Horozov, T. S.; Binks, B. P.; Johnston, K. P. Wetting phenomena at the CO₂/Water/Glass interface. *Langmuir* **2006**, *22*, 2161–2170.

(20) Cole, D. R.; Chialvo, A. A.; Rother, G.; Vlcek, L.; Cummings, P. T. Supercritical fluid behavior at nanoscale interfaces: Implications for CO₂ sequestration in geologic formations. *Philos. Mag.* **2010**, *90* (17–18), 2339–2363.

(21) Tripp, C. P.; Combes, J. R. Chemical modification of metal oxide surfaces in supercritical CO₂: The interaction of supercritical CO₂ with the adsorbed water layer and the surface hydroxyl groups of a silica surface. *Langmuir* **1998**, *14* (26), 7350–7352.

(22) McCool, B.; Tripp, C. P. Inaccessible hydroxyl groups on silica are accessible in supercritical CO₂. *J. Phys. Chem. B* **2005**, *109* (18), 8914–8919.

(23) Dickson, J. L.; Binks, B. P.; Johnston, K. P. Stabilization of carbon dioxide-in-water emulsions with silica nanoparticles. *Langmuir* **2004**, *20* (19), 7976–7983.

(24) Bikina, P. K. Contact angle measurements of CO₂-water-quartz/calcite systems in the perspective of carbon sequestration. *Int. J. Greenhouse Gas Control* **2011**, *5*, 1259–1271.

(25) Vishnyakov, A.; Shen, Y. Y.; Tomassone, M. S. Interactions of silica nanoparticles in supercritical carbon dioxide. *J. Chem. Phys.* **2008**, *129* (17), 174704.

(26) Liu, S. Y.; Yang, X. N.; Yan, Q. Molecular dynamics simulation of wetting behavior at CO₂/water/solid interfaces. *Chin. Sci. Bull.* **2010**, *55* (21), 2252–2257.

(27) Mahadevan, J. Comments on the paper titled "Contact angle measurements of CO₂-water-quartz/calcite systems in the perspective of carbon sequestration": A case of contamination? *Int. J. Greenhouse Gas Control* **2011**.

(28) Bikina, P. K. Reply to the comments on "Contact angle measurements of CO₂-water-quartz/calcite systems in the perspective of carbon sequestration. *Int. J. Greenhouse Gas Control* **2011**.

(29) Wan, J. M.; Tokunaga, T. K.; Tsang, C. F.; Bodvarsson, G. S. Improved glass micromodel methods for studies of flow and transport in fractured porous media. *Water Resour. Res.* **1996**, *32* (7), 1955–1964.

(30) Sohrabi, M.; Danesh, A.; Jamiolahmady, M. Visualisation of residual oil recovery by near-miscible gas and SWAG injection using high-pressure micromodels. *Transp. Porous Media* **2008**, *74* (2), 239–257.

(31) Mohammadzadeh, O.; Rezaei, N.; Chatzis, I. Pore-Level Investigation of Heavy Oil and Bitumen Recovery Using Solvent

-Aided Steam Assisted Gravity Drainage (SA-SAGD) Process. *Energy Fuels* **2010**, *24*, 6327–6345.

(32) Hatiboglu, C. U.; Babadagli, T. Pore-scale studies of spontaneous imbibition into oil-saturated porous media. *Phys. Rev. E* **2008**, *77* (6), 066311.

(33) Sharmin, R.; Ioannidis, M. A.; Legge, R. L. Effect of nonionic surfactant partitioning on the dissolution kinetics of residual perchloroethylene in a model porous medium. *J. Contam. Hydrol.* **2006**, *82* (1–2), 145–164.

(34) Sahloul, N. A.; Ioannidis, M. A.; Chatzis, I. Dissolution of residual non-aqueous phase liquids in porous media: Pore-scale mechanisms and mass transfer rates. *Adv. Water Resour.* **2002**, *25* (1), 33–49.

(35) Zhong, L. R.; Mayer, A.; Glass, R. J. Visualization of surfactant-enhanced nonaqueous phase liquid mobilization and solubilization in a two-dimensional micromodel. *Water Resour. Res.* **2001**, *37* (3), 523–537.

(36) Fenwick, D. H.; Blunt, M. J. Three-dimensional modeling of three phase imbibition and drainage. *Adv. Water Resour.* **1998**, *21* (2), 121–143.

(37) Wan, J. M.; Wilson, J. L. Visualization of the role of the gas-water interface on the fate and transport of colloids in porous-media. *Water Resour. Res.* **1994**, *30* (1), 11–23.

(38) Wan, J. M.; Wilson, J. L.; Kieft, T. L. Influence of the gas-water interface on transport of microorganisms through unsaturated porous-media. *Appl. Environ. Microbiol.* **1994**, *60* (2), 509–516.

(39) Wan, J. M.; Wilson, J. L. Colloid transport in unsaturated porous-media. *Water Resour. Res.* **1994**, *30* (4), 857–864.

(40) Guzman, K. A. D.; Finnegan, M. P.; Banfield, J. F. Influence of surface potential on aggregation and transport of titania nanoparticles. *Environ. Sci. Technol.* **2006**, *40* (24), 7688–7693.

(41) Baumann, T.; Toops, L.; Niessner, R. Colloid dispersion on the pore scale. *Water Res.* **2010**, *44* (4), 1246–1254.

(42) Auset, M.; Keller, A. A. Pore-scale visualization of colloid straining and filtration in saturated porous media using micromodels. *Water Resour. Res.* **2006**, *42* (12), W12S02.

(43) Grate, J. W.; Zhang, C. Y.; Wietsma, T. W.; Warner, M. G.; Anheier, N. C.; Bernacki, B. E.; Orr, G.; Oostrom, M. A note on the visualization of wetting film structures and a nonwetting immiscible fluid in a pore network micromodel using a solvatochromic dye. *Water Resour. Res.* **2010**, *46*, W1602.

(44) Riazi, M.; Sohrabi, M.; Jamiolahmady, M. Experimental Study of Pore-Scale Mechanisms of Carbonated Water Injection. *Transp. Porous Media* **2011**, *86* (1), 73–86.

(45) Wu, X.; Zhao, R.; Wang, R. Visual Experimental Study of the Factors Affecting the Stability of Foamy Oil Flow. *Pet. Sci. Technol.* **2011**, *29* (14), 1449–1458.

(46) Zhang, C.; Oostrom, M.; Grate, J. W.; Wietsma, T. W.; Warner, M. G. Liquid CO₂ Displacement of Water in a Dual-Permeability Pore Network Micromodel. *Environ. Sci. Technol.* **2011**, *45* (17), 7581–8.

(47) Riazi, M.; Sohrabi, M.; Bernstone, C.; Jamiolahmady, M.; Ireland, S. Visualization of mechanisms involved in CO₂ injection and storage in hydrocarbon reservoirs and water-bearing aquifers. *Chem. Eng. Res. Des.* **2011**, *89*, 1827–1840.

(48) Dawe, R. A.; Caruana, A.; Grattoni, C. A. Immiscible Displacement in Cross-Bedded Heterogeneous Porous Media. *Transp. Porous Media* **2011**, *87* (1), 335–353.

(49) Er, V.; Babadagli, T.; Xu, Z. H. Pore-Scale Investigation of the Matrix-Fracture Interaction During CO₂ Injection in Naturally Fractured Oil Reservoirs. *Energy Fuels* **2010**, *24*, 1421–1430.

(50) Rangel-German, E. R.; Kovscek, A. R. A micromodel investigation of two-phase matrix-fracture transfer mechanisms. *Water Resour. Res.* **2006**, *42* (3), W03401.

(51) Abramoff, M. D.; Magalhaes, P. J.; Ram, S. J. Image Processing with ImageJ. *Biophotonics Int.* **2004**, *11* (7), 36–42.

(52) Extrand, C. W.; Moon, S. I. Contact angles on spherical surfaces. *Langmuir* **2008**, *24* (17), 9470–9473.

(53) Marmur, A.; Krasovitski, B. Line tension on curved surfaces: Liquid drops on solid micro- and nanospheres. *Langmuir* **2002**, *18* (23), 8919–8923.

(54) Schiebener, P.; Straub, J.; Sengers, J.; Gallagher, J. S. Refractive-index of water and steam as function of wavelength, temperature and density. *J. Phys. Chem. Ref. Data* **1990**, *19* (3), 677–717.

(55) Sun, Y. D.; Shekunov, B. Y.; York, P. Refractive index of supercritical CO₂-ethanol solvents. *Chem. Eng. Commun.* **2003**, *190* (1), 1–14.

(56) Langmuir, I. Repulsive forces between charged surfaces in water, and the cause of the Jones-Ray effect. *Science* **1938**, *88*, 430–432.

(57) Buckingham, E. *Studies on the Movement of Soil Moisture*; Bureau of Soils, U. S. Department of Agriculture, Government Printing Office: Washington, DC, 1907.

(58) Hirasaki, G. J. Wettability: Fundamentals and surface forces. *SPE Form. Eval.* **1991**, June 1991, 217–226.

(59) Israelachvili, J. N. *Intermolecular and Surfaces Forces*, 2nd ed.; Academic Press: London, 1991; p 450.

(60) Vigil, G.; Xu, Z. H.; Steinberg, S.; Israelachvili, J. Interactions of Silica Surfaces. *J. Colloid Interface Sci.* **1994**, *165* (2), 367–385.

(61) Dove, P. M.; Craven, C. M. Surface charge density on silica in alkali and alkaline earth chloride electrolyte solutions. *Geochim. Cosmochim. Acta* **2005**, *69* (21), 4963–4970.

(62) Kaszuba, J. P.; Janecky, D. R.; Snow, M. G. Carbon dioxide reaction processes in a model brine aquifer at 200 degrees C and 200 bar: Implications for geologic sequestration of carbon. *Appl. Geochem.* **2003**, *18* (7), 1065–1080.

(63) Gribanova, E. V. Dynamic Contact Angles - Temperature-Dependence and the Influence of the State of the Adsorption Film. *Adv. Colloid Interface* **1992**, *39*, 235–255.

(64) Puah, L. S.; Sedev, R.; Fornasiero, D.; Ralston, J. Influence of Surface Charge on Wetting Kinetics. *Langmuir* **2010**, *26* (22), 17218–17224.

(65) Tokunaga, T. K. Physicochemical controls on adsorbed water film thickness in unsaturated geological media. *Water Resour. Res.* **2011**, *47*, W08514.

(66) Sghaier, N.; Prat, M.; Nasrallah, S. B. On the influence of sodium chloride concentration on equilibrium contact angle. *Chem. Eng. Sci.* **2006**, *122*, 47–53.

(67) Johansson, K.; Eriksson, J. C. γ and dy/dT measurements on aqueous solutions of 1,1-electrolytes. *J. Colloid Interface Sci.* **1974**, *49* (3), 469–480.

(68) Ralston, J.; Healy, T. W. Specific cation effects on water structure at air-water and air-octadecanol, monolayer-water interfaces. *J. Colloid Interface Sci.* **1973**, *42* (3), 629–644.

(69) Levin, Y.; dos Santos, A. P.; Diehl, A. Ions at the Air-Water Interface: An End to a Hundred-Year-Old Mystery? *Phys. Rev. Lett.* **2009**, *103* (25), 257802.

(70) Marcus, Y. Effect of Ions on the Structure of Water: Structure Making and Breaking. *Chem. Rev.* **2009**, *109* (3), 1346–1370.

(71) Tonnet, N.; Shah, V.; Chiquet, P.; Diaz, J.; Mouronval, G.; Broseta, D. Wettability alternation of caprock minerals by acid gases. Proceedings of the 10th International Symposium on Reservoir Wettability, Abu Dhabi, 26–28 October, 2008.